

Unexpected Values of Q_s in the Unconsolidated Sediments of the Mississippi Embayment

by Jose Pujol, Shahram Pezeshk, Ying Zhang, and Chengang Zhao

Abstract We studied the attenuation of shear waves at three sites in the Mississippi embayment using data recorded in boreholes drilled to depths of up to 60 m. The source was a highly repeatable compressed-air-driven hammer. To estimate attenuation we used a spectral ratio technique for fixed depth and variable frequency. The best-fit line for each depth z gives a measure of the cumulative attenuation, indicated by $\alpha(z)$. Then we fit a straight line to $\alpha(z)$ for a range of values of z . The slope of this line gives an estimate of the average attenuation per distance and was used to determine an average Q_s . For one of the sites (Newport, northeastern Arkansas), Q_s ranges between 34 ($1.5 \text{ m} \leq z \leq 44.2 \text{ m}$) and 44 ($1.5 \text{ m} \leq z \leq 51.8 \text{ m}$). These values are significantly higher than the more typical value of about 10 determined for unconsolidated sediments by other authors. In addition, these high values correspond to sediments with low average shear-wave velocity (about 300 m/sec). In contrast, average Q_s and velocity for sediments in Shelby Forest (near Memphis, Tennessee) are 22 and 348 m/sec ($22.6 \text{ m} \leq z \leq 60.1 \text{ m}$), respectively. Therefore, these results go against the conventional wisdom that low velocity implies low Q . For the third site (Marked Tree, northeastern Arkansas), average Q_s and velocity are 18 and 251 m/sec ($9.8 \text{ m} \leq z \leq 33.6 \text{ m}$), respectively. This site is about 75 km from Newport, and the differences in attenuation appear related to differences in lithology.

Introduction

As is well known (e.g., Field and the SCEC Phase III Working Group, 2000, and references therein), unconsolidated or poorly consolidated sediments amplify the ground motion caused by seismic waves significantly, thus increasing the damage they cause. This is one of the reasons why structures built in sedimentary basins are at a higher risk than those built on hard rock. On the other hand, seismic-wave attenuation in sediments can be high, which would contribute to a decrease in ground-motion amplitudes. Therefore, a reliable estimate of the seismic attenuation in this kind of environments is necessary for a realistic assessment of seismic hazard. This is particularly true for the New Madrid seismic zone, which is covered by the sediments of the Mississippi embayment, with a thickness of about 1 km near Memphis, Tennessee.

Attenuation is usually quantified in terms of the inverse of the quality factor Q , which, according to a number of studies, is quite low for some near-surface materials. We summarize relevant results in this article, but first, two comments are in order. First, because most of the damage to buildings and structures in an earthquake arises from horizontal forces, for seismic risk studies the quantity of interest is the Q for shear waves (Q_s). Second, the determination of reliable values of attenuation is difficult because wave amplitudes and shapes are affected by a number of factors other

than attenuation. For this reason we concentrate on studies that rely on in situ measurements conducted in boreholes, which are affected by the least amount of uncertainty.

Borehole attenuation studies are not common because of the costs of drilling and casing, and as a consequence, the number of published results appears to be small, particularly for near-surface materials and artificial sources. An early study is by Kudo and Shima (1970), who investigated attenuation in four boreholes about 40–50 m deep in Tokyo. Their average Q_s values are 5, 6.5, 8, and 20, depending on the nature of the soil and where determined for the depth intervals for which the soil layers were fairly uniform. More recently, several Q_s values corresponding to California sites have been reported. For example, for sands and gravel between 57 and 102 m and for alluvium between 10 and 115 m, average values of 4 and 10, respectively, have been determined (Gibbs and Roth, 1989; Gibbs *et al.*, 1994). A number of Q_s values obtained using earthquake data recorded in boreholes in California has been summarized by Abercrombie (1997). For depths up to 475 m, Q_s values range between 9 and 26 (the latter value corresponding to granite), with most values close to 10. In addition, recent modeling of site amplification in the Los Angeles region used a Q_s value of 10 for the 0- to 100-m depth range (Wald and Mori, 2000).

As described subsequently, the values of Q_s that we obtained range between 18 and 44, which are higher than most of the values reported previously. The significance of this difference may be assessed by considering how attenuation affects ground motion. To do that we simplified the velocity and density models derived by Dorman and Smalley (1994) from borehole and surface-wave data recorded in the Mississippi embayment. In their model, the P - and S -wave velocities in the poorly consolidated sediments are close to 1.8 and 0.6 km/sec, respectively, near the surface and reach about 3.0 and 1.4 km/sec, respectively, at 890 m. These low-velocity sediments are underlain by high-velocity dolomitic rocks, with P - and S -wave velocities of about 6.2 and 3.4 km/sec, respectively. From this model we generated two layer-over-half-space models, which were used to investigate the frequency response of a sedimentary layer to incident SH waves. The relevant equations are well known, but because a full derivation is not readily available, one is given in the Appendix, which also includes the modifications required to account for anelastic attenuation.

Figures 1 and 2 show the SH spectral ground motion for the two models referred to previously. The corresponding thicknesses and S -wave velocities are 0.1 km and 0.8 km/sec and 0.6 km and 1.0 km/sec, respectively. In both cases the S -wave velocity in the half-space was 3.35 km/sec. Without attenuation the ground motion can be amplified by a factor of about 5 with respect to the motion at a site without the layer (in which case the amplification is constant and equal to 2; see the Appendix). When a Q_s of 10 is used, the amplification can be greatly reduced for the lower periods. As expected, for a given period the attenuation increases with the thickness of the sediments. When the computations are repeated with a Q_s of 30, the effect of attenuation (not shown) is greatly reduced. For example, the amplitude of the left-most spectral peak in Figures 1 and 2 becomes close to 5 and 4, respectively. Although our modeling may oversimplify the problem, our results confirm that attenuation may be an important factor in seismic risk analysis depending on the values of Q_s and the periods of interest. Therefore, establishing the actual values of Q_s in the sediments of the Mississippi embayment will contribute to a better assessment of the seismic risk in the area.

Method to Determine Attenuation

The determination of attenuation is based on the standard assumption of exponential amplitude decay in the frequency domain. For the case of borehole data and a seismic source close to the borehole the variation in wave amplitudes can be represented by the following relation:

$$A_z(f) = (G_0/G_z) e^{-\alpha f} A_0(f) \quad (1)$$

where $A_0(f)$ is the amplitude of a reference wavelet at depth z_0 , $A_z(f)$ is amplitude of a wavelet at depth z , α is the atten-

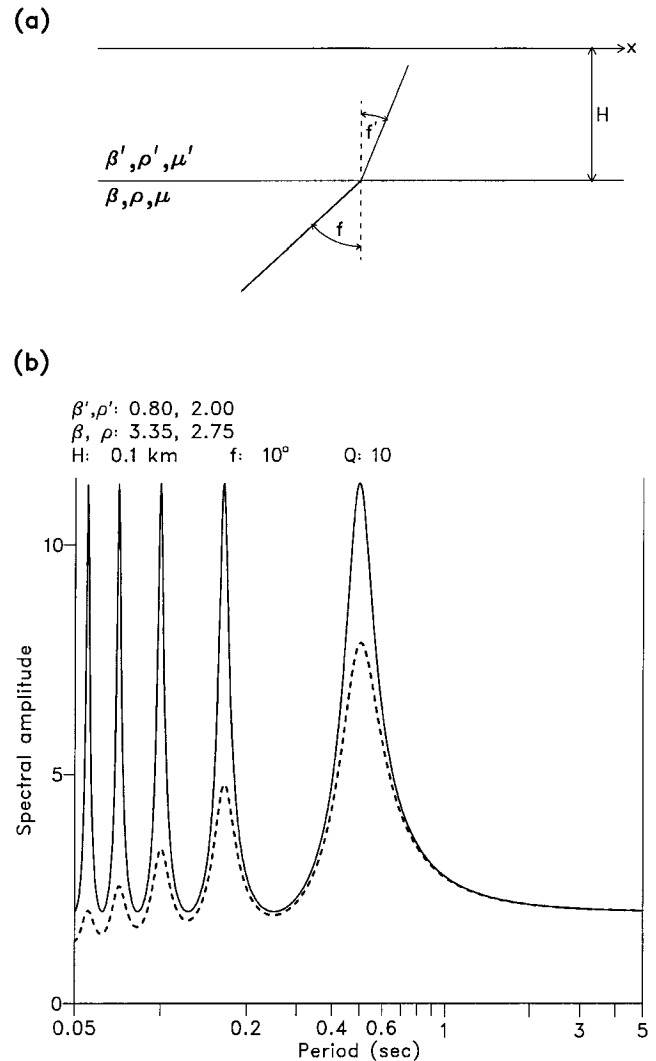


Figure 1. (a) Parameters of the layer-over-half-space model used for the analysis of SH waves incident at the bottom of the layer. β , ρ , and μ indicate S -wave velocity, density, and rigidity, respectively, for the half-space. Primed symbols correspond to the layer. H is layer thickness, and f is incidence angle. (b) Spectral amplitude vs. period for SH waves for the model shown in (a). The velocity and density in the layer and in the half-space are 0.80 km/sec and 2.00 gm/cm³ and 3.35 km/sec and 2.75 gm/cm³, respectively. The layer thickness is 0.1 km. These values roughly represent the unconsolidated sediments of the Mississippi embayment and the underlying Paleozoic rocks near the northern end of the embayment. The incidence angle is 10°. The solid line corresponds to the absolute value of the ground displacement as a function of period, computed using equation (A19) with $C_u = 1$. The dashed line shows the effect of attenuation (introduced using equation A33 with $Q' = 10$) on the ground displacement.

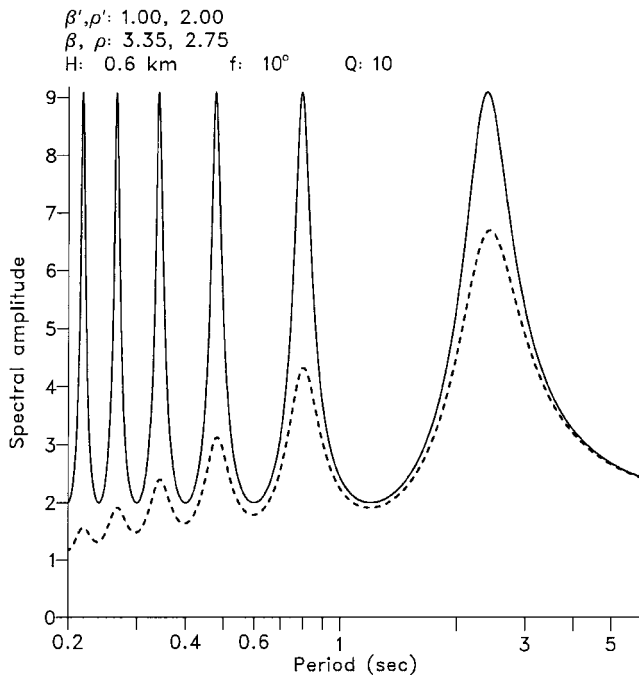


Figure 2. Similar to Figure 1b. The only differences are in the layer thickness and velocity, equal to 0.6 km and 1.00 km/sec respectively. This model roughly corresponds to the Mississippi embayment near the northern end of the central segment of the New Madrid seismic zone.

uation coefficient, and G_0 and G_z are frequency-independent geometric spreading factors for depths z_0 and z . Of course, this model does not consider a number of factors that affect wave amplitudes and shapes, such as fine layering, reflections and transmission effects when layers are present, scattering, coupling of the receiver to the borehole, and source variations (e.g., Hauge, 1981; Pujol and Smithson, 1991). Of all these factors, fine layering may be the most serious because its effect mimics the intrinsic attenuation modeled by (1), so it may be difficult to separate the two effects. The other factors have effects that are more obvious, and it is possible to establish when they are so important that they affect the reliability of the results. The results presented in this article illustrate this point. Regarding possible source variations, it is convenient to have a receiver at a fixed position recording the waves generated each time that the source is activated. Then the data recorded with this source monitor can be used to extract A_0 . Another possible source of error is introduced by the use of a time-domain window to isolate the wavelet to be analyzed. This process, known as windowing, is discussed subsequently.

When the medium is homogeneous, α is given by

$$\alpha = \pi \delta z / Qv \quad (2a)$$

$$\delta z = z - z_0, \quad (2b)$$

where v is the velocity of wave propagation in the medium. If α is independent of frequency, then one way to estimate Q is to fix z , to divide (1) by A_0 , and then to take logarithms on both sides. This gives

$$\ln \frac{A_z(f)}{A_0(f)} = -\alpha(z)f + \ln \frac{G_0}{G_z}, \quad (3)$$

which is the equation of a straight line in f . In this context α is a function of z , known as cumulative attenuation, and can be determined by fitting a least-squares line to the observations. Once $\alpha(z)$ has been computed, Q as a function of depth can be estimated using (2a). However, as scatter in the data may preclude the determination of reliable values of Q , we fit a straight line to $\alpha(z)$ for a range of values of z . Let k be the slope of the best-fit line. Then, from (2a) we get

$$k = \frac{\pi}{vQ}, \quad (4)$$

so that

$$Q = \frac{\pi}{vk}, \quad (5)$$

and

$$\alpha = k\delta z. \quad (6)$$

The Q value determined using (5) is an average value, and if $\alpha(z)$ is an approximately piecewise linear function of z , there will be a pair of values k and Q for each segment.

This method is based on that of Hauge (1981) and is convenient because it is not necessary to know the true amplitudes of the waves. When the assumption that α is independent of f is not valid, an alternative method is to fix f and let z vary (Pujol and Smithson, 1991). In this case it is critical to account for the geometric spreading correctly.

To estimate the standard deviation σ_Q of Q , we use

$$\sigma_Q = \left| \frac{dQ}{dk} \right| \sigma_k = \frac{Q}{k} \sigma_k \quad (7)$$

(Pujol and Smithson, 1991), where σ_k is the standard deviation of k , computed from

$$\sigma_k^2 = \frac{\sigma^2}{\sum_{i=1}^N (z_i - \bar{z})^2}, \quad (8)$$

where N is the number of values $\alpha(z_i)$, \bar{z} is the average of the depths z_i , and σ is the standard deviation of the errors in the data being fitted, estimated using

$$\sigma^2 = \frac{1}{N-2} \sum_{i=1}^N [\alpha(z_i) - kz_i - b]^2, \quad (9)$$

where b is the intercept of best-fit line (Jenkins and Watts, 1968).

The effect of windowing on the estimation of Q was discussed by Pujol and Smithson (1991), who showed that if $\mathcal{A}_z(f) = A_z(f)\exp[i\phi(f)]$ and $\mathcal{A}_0(f)$ are the Fourier transforms of the wavelets at depths z and z_0 and $\mathcal{W}(f)$ is the Fourier transform of the windowing function, then the ratio actually used in (3) is

$$\frac{|\mathcal{A}_z(f) * \mathcal{W}(f)|}{|\mathcal{A}_0(f) * \mathcal{W}(f)|} = \frac{A_z(f)}{A_0(f)} \frac{|[A_0(f)e^{i\phi(f)}] * [e^{\alpha f}\mathcal{W}(f)]|}{|\mathcal{A}_0(f) * \mathcal{W}(f)|}, \quad (10)$$

where the convolutions arise because the window multiplies the wavelets in the time domain.

Equation (10) shows that the desired amplitude ratio (i.e., $\mathcal{A}_z/\mathcal{A}_0$) appears multiplied by a complicated function that depends on the wavelets, the window, and the attenuation coefficient. As Harris *et al.* (1997) noted, the factor $\exp(\alpha f)$ increases with frequency, and for this reason it is important that the sidelobes of $\mathcal{W}(f)$ have small amplitudes. From the analysis of synthetic data (Pujol and Smithson, 1991; Wilson, 1990) it was found that the computed values of Q may show a spurious dependence on f , which in turn is a function of the type and length of the window used.

For the data discussed in this article, the waveforms are quite simple, and for this reason the portion of data used in the attenuation analysis was obtained by truncation at points where the wave amplitudes are zero (or close to it). Under these conditions the discrete Fourier transform is equal to the continuous transform (within a scale factor). The lobes in the transform of the rectangular window we used are not a factor because their only contributions to the discrete transform are those with amplitudes equal to zero (Brigham, 1974, p. 102). Application of this window was the only data processing technique employed, which means that the remarkable smoothness of the spectra and spectral ratios shown in subsequent figures is inherent in the data.

Data

Three data sets were analyzed. One of them was recorded in a 60-m borehole near the town of Newport, Arkansas, about 125 km to the west-northwest of Memphis. The borehole was drilled in 1998, cased with 3-inch inner diameter polyvinyl chloride pipe and grouted from the bottom up. The seismic source was a shear-wave generator similar to that described by Liu *et al.* (1996, 1997). Basically, it consists of a compressed-air-driven hammer that slides on low-friction tracks. The hammer impacts on two anvils located on both sides of the hammer. The two impacts correspond to the forward and retracting motions of the ham-

mer. The weight of a truck on the source gives a good coupling to the ground. The source was built by personnel of the Department of Civil Engineering at The University of Memphis.

A three-component 8-Hz geophone was placed in the borehole at 1.5-m (5-ft) intervals to a depth of 60 m. The time sampling interval was 0.67 msec. A pneumatic packer pumped from the surface was used to clamp the geophone to the borehole. The source was located about 1 m from the borehole and was monitored with a three-component 4.5-Hz geophone placed on the surface about 1 m from the source. For each depth position four traces were recorded, two for each of the hammer directions. As discussed by Liu *et al.* (1997), the clamping device may have a filtering effect on the recorded waveforms depending on the relative positions of the horizontal geophones with respect to the clamping device. This effect was noticed in our data, and for this reason we did not stack the traces corresponding to the same depth. In addition, because our analysis did not use true amplitudes, the traces were not rotated to maximize the energy in one of the rotated components (e.g., Di Siena *et al.*, 1984).

The collection of traces recorded at different depths in a borehole is known as a vertical seismic profile (VSP). The VSP traces corresponding to one of the horizontal components of the Newport data, and the respective monitor traces are shown in Figure 3. A few deeper traces affected by noise were discarded. All the traces have been normalized so that the largest amplitude in each trace is one. Aside from a minor increase in high-frequency amplitudes (see next section), the monitor traces show that the seismic source is highly repeatable. For this reason, the major variations seen in the shape of the VSP traces are due to changes in the elastic properties of the medium (i.e., velocity, density) and/or changes in recording conditions. One possible cause for variation is the rotation (which cannot be controlled) of the geophone when it is moved from one depth to the next so that the position of a given component is not fixed with respect to the source. Another possible cause is a variation in the casing-formation coupling, which depends on the quality of the grouting. In places where the grouting is poor the coupling of the geophone to the ground will also be poor, which may introduce noise into the waveforms (Gal'perin, 1974; Hardage, 1985).

The two other data sets were recorded in boreholes drilled in Marked Tree, Arkansas, about 60 km northwest of Memphis and about 75 km to the east of Newport, and in Shelby Forest, about 25 km to the north of Memphis (Liu *et al.*, 1997). In both cases the geophone spacing was 0.9 m (3 ft), and the time sampling interval was 3.33 msec. Although reference geophones were used, the corresponding monitor traces were not available to us. Figures 4 and 5 show the recorded traces after vertical stacking of all the traces for a given depth. The Shelby Forest data were recorded to a depth of 60 m, and because for the upper 22 m the traces were quite complicated, only the bottom traces were used.

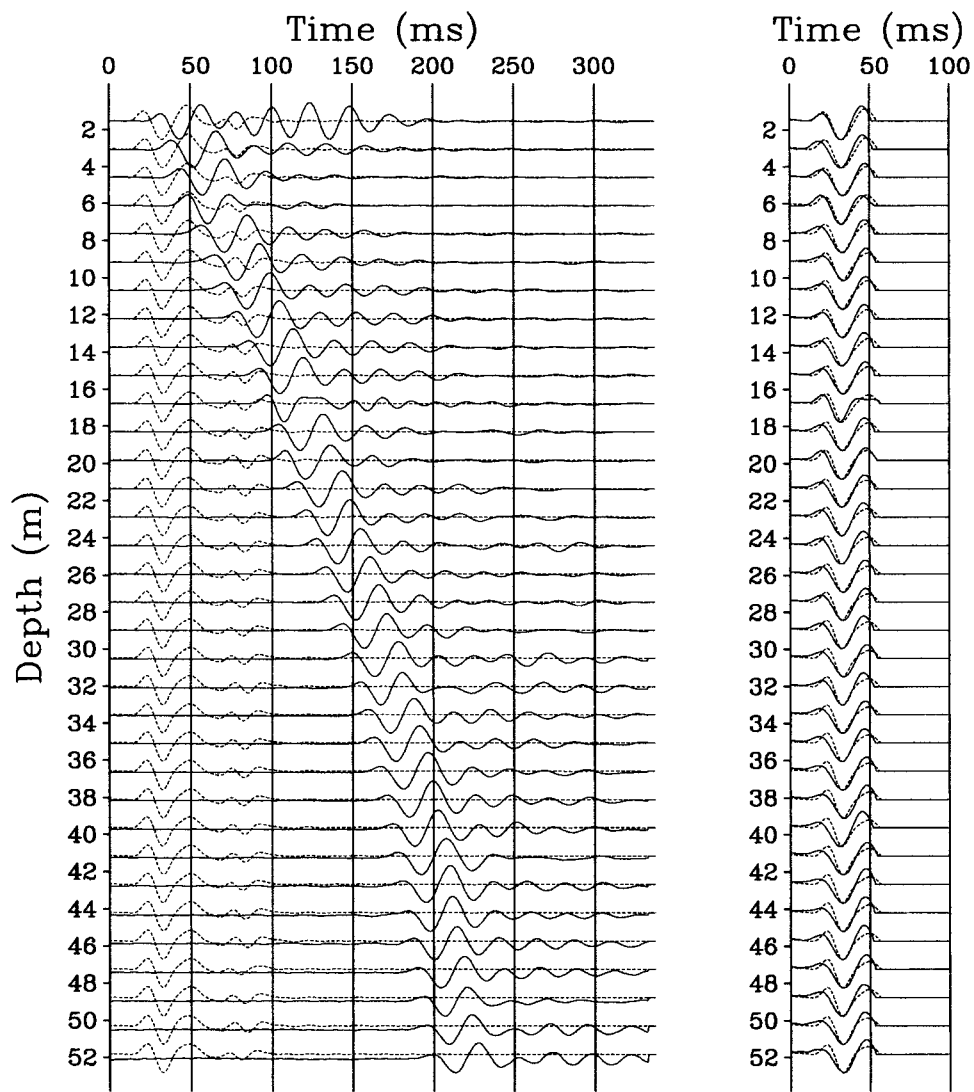


Figure 3. (Left) VSP traces recorded in the Newport, Arkansas, borehole (solid lines) and corresponding monitor traces (dashed lines). (Right) First cycle of the traces on the left used for the attenuation analysis.

Data Analysis

Figure 3 shows the Newport traces after truncation and time shifting to align their first peak. The spectra of the VSP and monitor traces are shown in Figure 6. Note the effect of attenuation on the spectral content of the VSP traces, namely, an increasing reduction in amplitude with depth for the higher frequencies, and a corresponding shift of the peak frequencies to lower values, as expected for the attenuation model given by equation (1) (Pujol and Smithson, 1991). The monitor traces, on the other hand, show an increase in amplitude for the higher frequencies as the depth increases. Because the experiment was conducted from the surface down and the source position was unchanged, the amplitude increase for the higher frequencies is probably the result of a source-ground coupling that kept improving as the exper-

iment proceeded. The spectral ratios (Fig. 6) show a linear relation between 10 and 50 Hz only. The drastic change in slope at about 10 Hz is probably due to the use of different types of geophones for the monitor and borehole recordings. We applied a correction to the VSP data based on the theoretical instrument responses, but it appears that it was not successful for the lower frequencies.

The slopes $\alpha(z)$ of the straight lines fit to the attenuation curves (see Fig. 6) are plotted versus depth in Figure 7. As expected, $\alpha(z)$ follows an increasing trend with depth, with the observed scatter caused by one or more of the various factors affecting wave amplitudes and shapes mentioned previously. The uncertainties in α , computed using an expression similar to (8), are much smaller than the scatter (Fig. 7). Because of this scatter some points were ignored in the computation of the best-fit line. The slope k of this line is

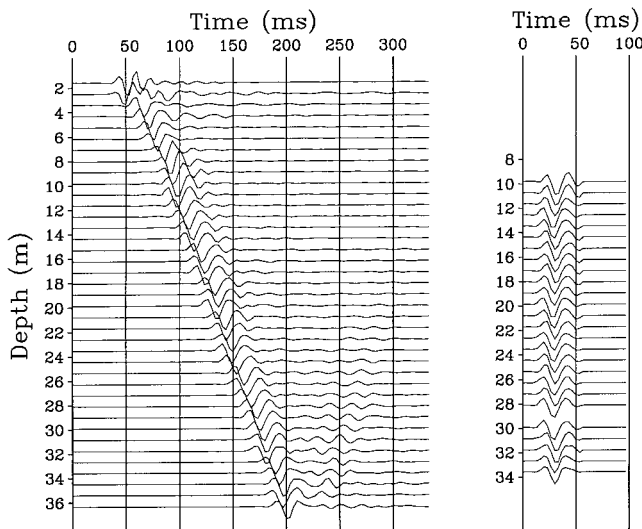


Figure 4. (Left) VSP traces recorded in the Marked Tree, Arkansas, borehole. (Right) First cycle of the traces on the left used for the attenuation analysis.

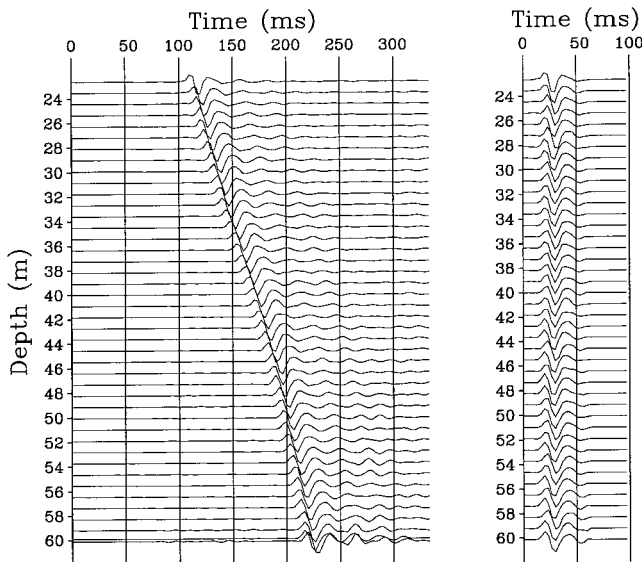


Figure 5. (Left) VSP traces recorded in the Shelby Forest (near Memphis) borehole. (Right) First cycle of the traces on the left used for the attenuation analysis.

0.31×10^{-3} . For an average velocity of 300 m/sec, we get a Q_s value of 34 ± 6 . When the deepest five points are also included in the computations, k and Q_s are given by 0.24×10^{-3} and 44 ± 9 , respectively. The corresponding depth intervals are 1.5–44.2 m and 1.5–51.8 m.

Because a monitor geophone was not available for the other two data sets, we repeated the computations for the Newport data using the trace recorded at a depth of 3 m for the computation of A_0 . Also in this case data from the five deepest traces were not used. The corresponding results are

shown in Figures 8 and 9. The most interesting differences with the previous results are a somewhat larger scatter, a smaller value of k (equal to 0.24×10^{-3}), and a larger value of Q_s (equal to 44 ± 11). This difference in Q_s values is due to the increase in the amplitude of the monitor traces for the higher frequencies noted before. If these traces are treated as VSP traces, the slope k is -0.7×10^{-4} . When this number is subtracted from k for the actual data the resulting value is 0.31×10^{-3} , which is equal to the value of k obtained when the monitor traces were used to compute A_0 .

The results for the Marked Tree and Shelby Forest data are presented in Figures 10 and 11 and 12 and 13. For the Marked Tree data the depth range is 9.8–33.6 m, the scatter is larger than for the Newport data, k is equal to 0.70×10^{-3} , and the Q_s computed for an average velocity of 251 m/sec is equal to 18 ± 4 . Although this data set is not the most appropriate for attenuation studies, it is included for comparison with the Newport results. For the Shelby Forest data the depth range is 22.6–60.1 m, the amount of scatter is the least, k is equal to 0.41×10^{-3} , and Q_s computed for an average velocity of 348 m/sec is equal to 22 ± 2 .

The uncertainties in Q given here are computed assuming that the velocity v is known exactly. To estimate the error introduced by an inexact knowledge of v , Q was computed with the values of v modified by $\pm 10\%$, which translates into errors in Q of about ± 4 for the Newport borehole and about ± 2 for the two other boreholes.

Discussion

In view of the values reported in the Introduction, the Q_s determined for the Newport borehole, ranging between 34 and 44 (depending on the depth range analyzed) is unexpected and should change our view of how much attenuation can be expected in shallow sediments. In particular, the association of very low v_s and relatively high Q_s goes against the conventional wisdom that Q_s should also be low. The Newport data are also useful because they have shown the importance of using monitor data to account for any source variations that may exist. In this particular case, ignoring these variations results in a value of Q_s overestimated by about 30%. As the two other VSPs were also conducted from the surface to the bottom of the borehole (H.-P. Liu, 2001, personal comm) the corresponding Q_s values may be overestimated if the source-ground coupling improved during the experiments.

The Marked Tree data, although affected by more scatter than the Newport data, are important because the two boreholes are relatively close to each other and yet have significantly different Q_s values. The lines labeled $Q = 15$ in Figures 7 and 11 have been drawn to emphasize this difference in attenuation: while this line is within the scatter of the Marked Tree data, it is well above the Newport data. Also note that the scatter in the two data sets prevents the determination of reliable values of Q_s as a function of depth

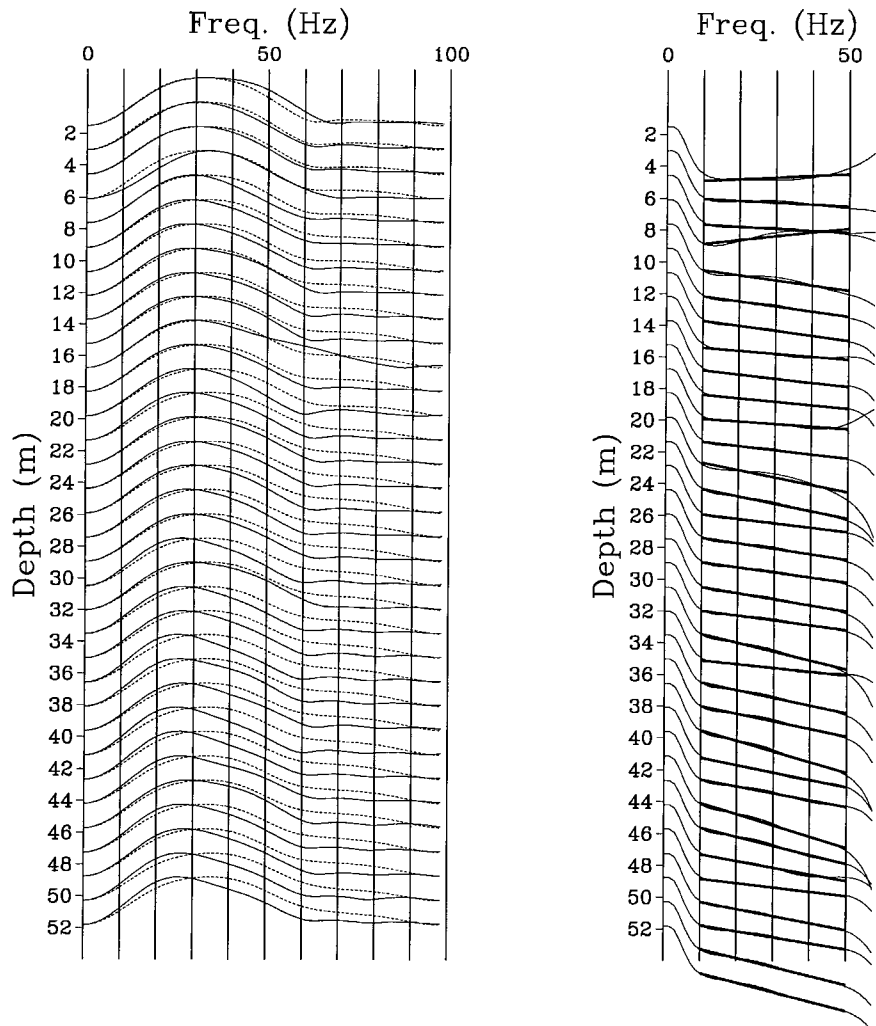


Figure 6. (Left) Normalized amplitude spectra for the Newport data obtained from analysis of the first cycles of Figure 3. The continuous and dashed lines correspond to the VSP and monitor traces, respectively. (Right) Spectral ratios obtained using the left side of equation (3) with A_0 being the spectrum of the corresponding monitor trace. The best-fit least-squares lines in the 10- to 50-Hz range are also shown. The slope of each line gives $\alpha(z)$.

but that in both cases α shows a clear linear increase, with the slope of the best-fit line giving a more realistic assessment of the attenuation experienced by the waves over the depth range considered. This in turn means that the exponential decay is probably better represented with α given by equation (6) rather than by (2a).

Regarding the cause of the difference in Q_s values for these two boreholes, it must be related to the differences in lithology. As described in Liu *et al.* (1997), the Marked Tree borehole was drilled in fluvial, floodplain deposits, with three layers of medium to coarse sands with sandy clay lenses between about 10 and 15 m, followed by a 3-m-thick layer of medium to coarse sand with occasional rounded gravel, followed by layers of fine to coarse sands, gravelly and abundant lignite. The lithology at the Newport site is very different. Down to a depth of about 15 m there are seven

layers of medium-dense to dense silt, clayey silt, sandy silt, and silty clay, followed by the following sections (the numbers in parentheses give the depth range): dense medium to coarse sand (15–27 m), dense medium to coarse sand with some fine to coarse gravel (27–37 m), dense medium to coarse sand with some fine gravel and coarse gravel (37–48 m), and very stiff clay with silty sand seams and partings (48–60 m). These differences in lithology at the two sites appear to be responsible for the observed difference in attenuation.

As noted previously, the Shelby Forest data (Figs. 12 and 13) are affected by the least amount of scatter, which is consistent with less variation in the lithology. In the depth range considered in this article, the sediments are shallow marine clay, sand, and silt deposits (Liu *et al.*, 1997). The obvious changes in the value of $\alpha(z)$ slightly below 40 m in

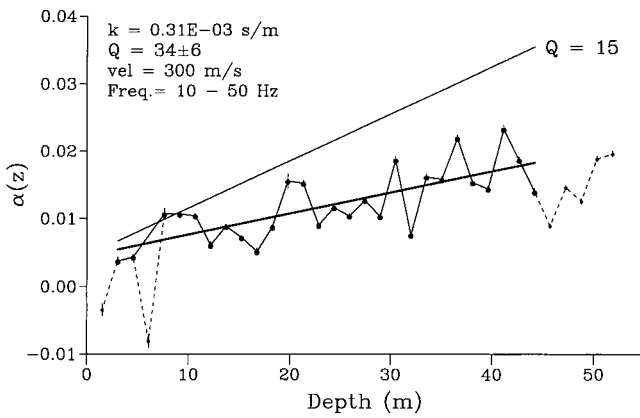


Figure 7. Attenuation curve for the Newport data. Dots represent the cumulative attenuation $\alpha(z)$ (in sec; see Fig. 6), and the associated short segments indicate plus or minus one standard deviation. A dashed line joins all the values of α , whereas the solid broken line joins the values used to determine the slope k by fitting a straight line (bold line). The line labeled $Q = 15$ has been drawn for comparison with Figures 11 and 13.

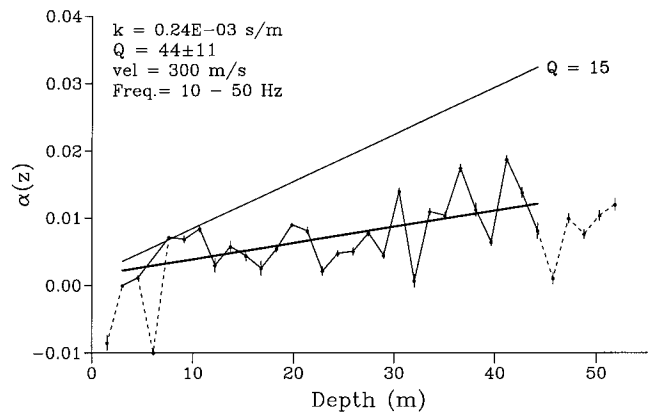


Figure 9. Attenuation curve for the Newport data with $\alpha(z)$ derived from the spectral ratios in Figure 8. Other features as in Figure 7.

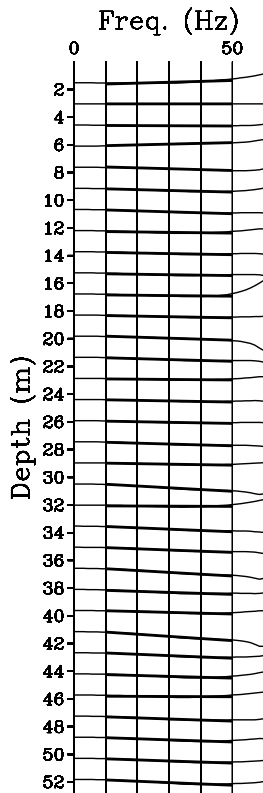


Figure 8. Spectral ratios for the Newport data obtained from analysis of the first cycles of Figure 3. Equation (3) was used with the spectra shown in Figure 6 and A_0 being the spectrum of the trace recorded at a depth of 3 m. The best-fit least-squares lines in the 10- to 50-Hz range are also shown.

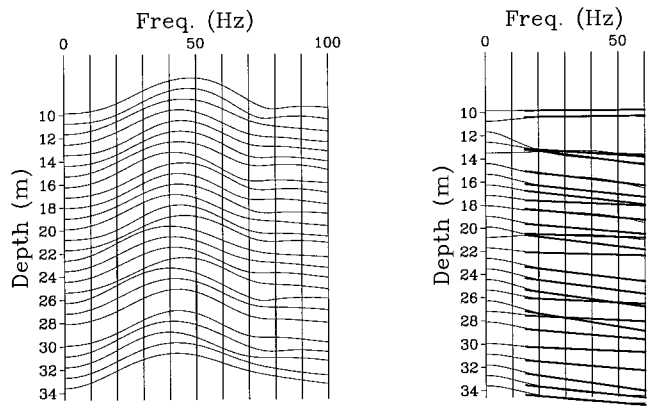


Figure 10. (left) Normalized amplitude spectra for the Marked Tree data obtained from analysis of the first cycles of Figure 4. (Right) Spectral ratios obtained using equation (3) with A_0 being the spectrum of the trace recorded at a depth of 9.8 m. The best-fit least-squares lines in the 15- to 60-Hz range are also shown.

Figure 13 agrees with a change from a clay layer to a sand layer. Interestingly, although k for this data set is 41% smaller than for the Marked Tree data, the difference in Q_s values is 19%. This is another reason why k is a more useful indicator of attenuation than Q_s . Comparison of results for the Shelby Forest and Newport boreholes (Figs. 7 and 13) shows that attenuation in the former is significantly higher than in the latter.

Conclusions

The most significant result of our attenuation analysis is that Q_s for shallow (≈ 60 m or less) Mississippi embayment sediments is between 18 and 34–44, the latter values depending on the depth range analyzed. These values are larger, or much larger, than most of the values reported in

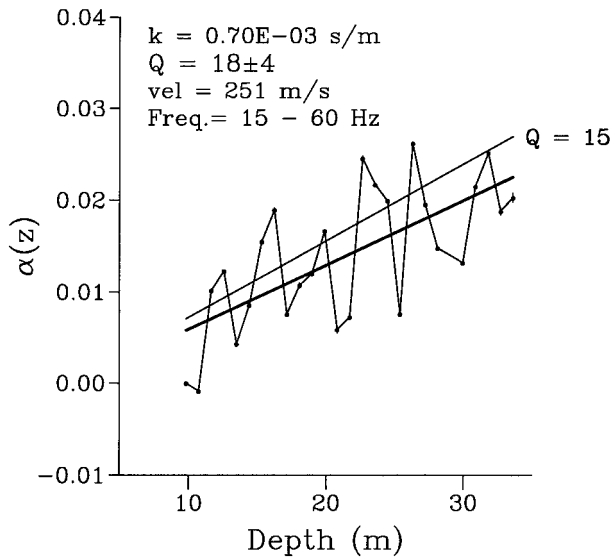


Figure 11. Attenuation curve for the Marked Tree data with $\alpha(z)$ derived from the spectral ratios in Figure 10. Other features as in Figure 7.

the literature, which are around 10. This difference is clearly important because of their bearing on ground amplification in the case of an earthquake. Although our results are limited to frequencies higher than 10–20 Hz, they are potentially significant for seismic hazards analysis because they are close to the resonant frequencies of one-story buildings. A necessary follow-up step is to try to extend our analysis to

lower frequencies. This will require experiments specifically designed for attenuation studies, with emphasis in source monitoring. As the analysis of the Newport data shows, recording of the source signature allowed us a more reliable determination of attenuation, and should be a standard feature of in situ attenuation studies.

Our results also show that low velocity does not necessarily imply low Q , as is generally assumed, and also confirm the known fact that attenuation depends on the combination vQ , rather than just Q . Although Q is a very convenient parameter, the slope k gives a more accurate view of the amount of attenuation and thus it is more useful to quantify attenuation. Moreover, when the layering is such that reflection and transmission effects are important, the ensuing scatter in the attenuation curves may preclude the determination of realistic values of Q as a function of depth. In such cases attenuation is better estimated through k .

Acknowledgments

The acquisition of the Newport borehole data was supported by a grant from the Tennessee Dept. of Transportation to S. Pezeshk. We are grateful to the late H.-P. Liu (USGS) for providing the blueprints of the shear-wave source and for his permission to use the Shelby Forest and Marked Tree data. We thank an anonymous reviewer for constructive comments and Dr. S. Harmsen for identifying an error in the way we had initially accounted for attenuation in Figures 1 and 2. The work reported in this article was supported by the Earthquake Engineering Research Centers Program of the National Science Foundation under Award Number EEC-9701785 and by the State of Tennessee Centers of Excellence program. This is CERI Contribution Number 432.

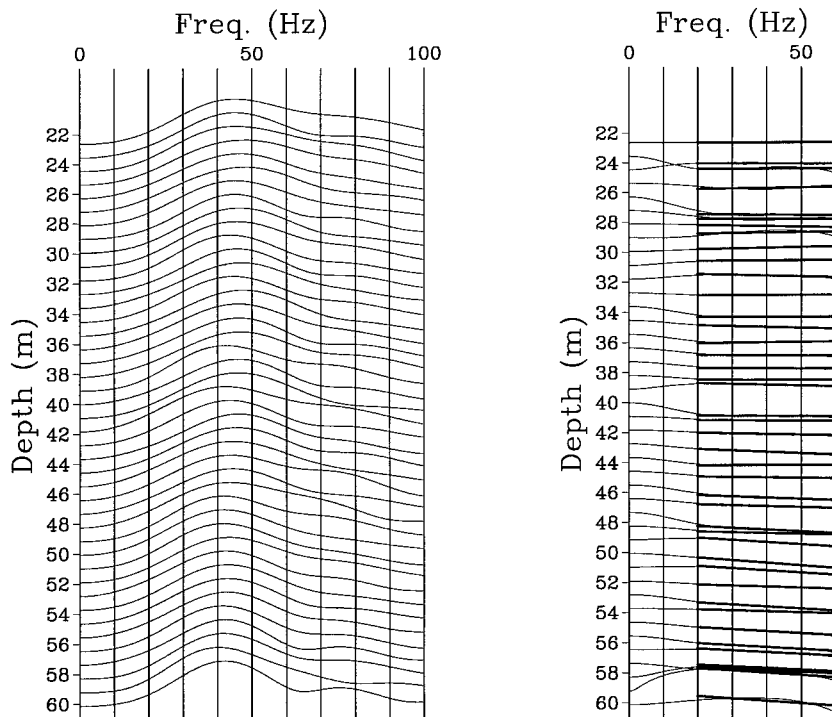


Figure 12. (Left) Normalized amplitude spectra for the Shelby Forest data obtained from analysis of the first cycles of Figure 5. (Right) Spectral ratios obtained using equation (3) with A_0 being the spectrum of the trace recorded at a depth of 22.6 m. The best-fit least-squares lines in the 20- to 60-Hz range are also shown.

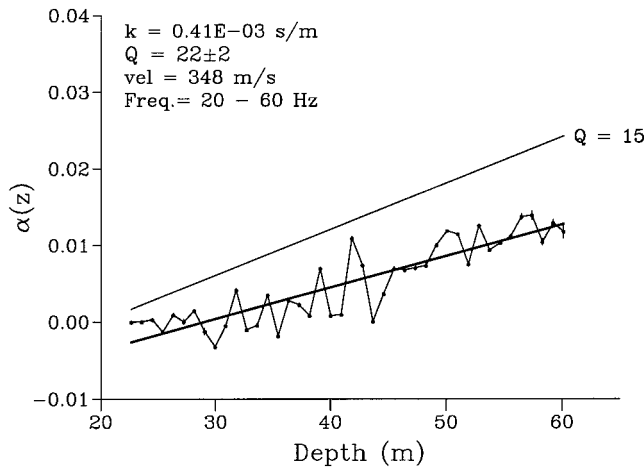


Figure 13. Attenuation curve for the Shelby Forest data with $\alpha(z)$ derived from the spectral ratios in Figure 12. Other features as in Figure 7

References

- Abercrombie, R. (1997). Near-surface attenuation and site effects from comparison of surface and deep borehole recordings, *Bull. Seism. Soc. Am.* **87**, 731–744.
- Ben Menahem, A., and S. Singh (1981). *Seismic Waves and Sources*, Springer Verlag, New York.
- Boore, D., and L. Brown (1998). Comparing shear-wave velocity profiles from inversion of surface-wave phase velocities with downhole measurements: systematic differences between the CXW method and downhole measurements at six USC strong-motion sites, *Seism. Res. Lett.* **69**, 222–229.
- Brigham, E. (1974). *The Fast Fourier Transform*, Prentice-Hall, Englewood Cliffs, New Jersey.
- Di Siena, J., J. Gaiser, and D. Corrigan (1984). Analyzing three-component data in *Vertical Seismic Profiling*, Part B, M. Töksoz and R. Stewart (Editors), Geophysical Press, London, 177–188.
- Dorman, J., and R. Smalley (1994). Low-frequency seismic surface waves in the upper Mississippi embayment, *Seism. Res. Lett.* **65**, 137–148.
- Field, E., and the SCEC Phase III Working Group (2000). Accounting for site effects in probabilistic seismic hazard analyses of southern California: overview of the SCEC Phase III working group, *Bull. Seism. Soc. Am.* **90**, S1–S31.
- Ganley, D. (1981). A method for calculating synthetic seismograms that include the effects of absorption and dispersion, *Geophysics* **46**, 1100–1107.
- Gal'perin, E. (1974). *Vertical Seismic Profiling*, Soc. Expl. Geophysicists Special Pub. no. 12, Society of Exploration Geophysicists, Tulsa, Oklahoma.
- Gibbs, J., and E. Roth (1989). Seismic velocities and attenuation from borehole measurements near the Parkfield prediction zone, central California, *Earthquake Spectra* **5**, 513–537.
- Gibbs, J., D. Boore, W. Joyner, and T. Fumal (1994). The attenuation of seismic shear waves in quaternary alluvium in Santa Clara valley, California, *Bull. Seism. Soc. Am.* **84**, 76–90.
- Hardage, B. (1985). *Vertical Seismic Profiling*, Part A, Geophysical Press, London.
- Harris, P., C. Kerner, and R. White (1997). Multichannel estimation of frequency-dependent Q from VSP data, *Geophys. Prosp.* **45**, 87–109.
- Haskell, N. (1960). Crustal reflections of plane SH waves, *J. Geophys. Res.* **65**, 4147–4150.
- Hauge, P. S., (1981). Measurements of attenuation from vertical seismic profiles, *Geophysics* **46**, 1548–1558.

- Jenkins, G., and D. Watts (1968). *Spectral Analysis and Its Applications*, Holden-Day, San Francisco.
- Kanai, K. (1957). The requisite conditions for the predominant vibration of ground, *Bull. Earthquake Res. Inst.* **35**, 457–471.
- Kudo, K., and E. Shima (1970). Attenuation of shear waves in soil, *Bull. Earthquake Res. Inst.* **48**, 145–148. Reprinted in *Seismic Wave Attenuation*, M. Toksöz and D. Johnston (Editors), Society of Exploration Geophysicists, Tulsa, Oklahoma, Geophysics reprint series, no. 2, 325–338.
- Liu, H.-P., Y. Hu, J. Dorman, T.-S. Chang, and J.-M. Chiu (1997). Upper Mississippi embayment shallow seismic velocities measured in situ, *Eng. Geology* **46**, 313–330.
- Liu, H.-P., R. Maier, and R. Warrick (1996). An improved air-powered impulsive shear-wave source, *Bull. Seism. Soc. Am.* **86**, 530–537.
- Pujol, J., and S. Smithson (1991). Seismic wave attenuation in volcanic rocks from VSP measurements, *Geophysics* **56**, 1441–1455.
- Wald, L., and J. Mori (2000). Evaluation of methods for estimating linear site-response magnification in the Los Angeles region, *Bull. Seism. Soc. Am.* **90**, S32–S42.
- Wiechert, E., and K. Zoeppritz (1907). Über Erdbebenwellen, *Nachrichten Königl. Gesell. Wissenschaften zu Göttingen*, 427–469.
- Wilson, A. (1990). Computer software for the processing and interpretation of VSP data including the study of seismic wave attenuation, *M.S. Thesis*, Memphis State University, Memphis, Tennessee.

Appendix

SH Waves in a Layer over a Half-Space

The displacement in the layer, written in component form and indicated by v' , is given by

$$v' = C'_u \exp \left[i\omega \left(t - x \frac{\sin f'}{\beta'} + z \frac{\cos f'}{\beta'} \right) \right] + C'_d \exp \left[i\omega \left(t - x \frac{\sin f'}{\beta'} - z \frac{\cos f'}{\beta'} \right) \right] \quad (\text{A1})$$

(Ben-Menahem and Singh, 1981). The model parameters are shown in Figure 1. The first and second terms on the right represent waves going up and down, respectively. The equation for the displacement in the half-space is similar to (A1) with all the primed quantities replaced by their unprimed counterparts, but before writing it a few notational changes and simplifications will be introduced. Using Snell's law,

$$c = \frac{\beta}{\sin f} = \frac{\beta'}{\sin f'}, \quad (\text{A2})$$

where c is the phase velocity along the boundary and $k = \omega/c$, we have

$$\omega \frac{\sin f}{\beta'} = \omega \frac{\sin f'}{\beta'} = k \quad (\text{A3})$$

and

$$\omega \frac{\cos f'}{\beta'} = \frac{\omega}{\beta'} \sqrt{1 - \sin^2 f'} = \frac{\omega}{c} \sqrt{\frac{c^2}{\beta'^2} - 1} = k\eta' \quad (\text{A4})$$

with

$$\eta' = \begin{cases} \sqrt{\frac{c^2}{\beta'^2} - 1}, & \text{if } c > \beta' \\ -i \sqrt{1 - \frac{c^2}{\beta'^2}}, & \text{if } c < \beta'. \end{cases} \quad (\text{A5a,b})$$

There is a similar equation for η with β' replaced by β . The choice of sign in (A5b) is not critical, as $c \geq \beta$ in the layer. With these definitions and temporarily ignoring the common factor $\exp[i(\omega t - kx)]$, the displacements in the layer and in the half-space can be written as

$$v' = C'_u e^{izk\eta'} + C'_d e^{-izk\eta'} \quad (\text{A6})$$

and

$$v = C_u e^{izk\eta} + C_d e^{-izk\eta}. \quad (\text{A7})$$

The corresponding stress components are given by

$$\tau_{32} = \mu' \frac{\partial v'}{\partial z} = i\mu' k\eta' (C'_u e^{izk\eta'} - C'_d e^{-izk\eta'}) \quad (\text{A8})$$

and

$$\tau_{32} = \mu \frac{\partial v}{\partial z} = i\mu k\eta (C_u e^{izk\eta} - C_d e^{-izk\eta}). \quad (\text{A9})$$

In these equation C_u is assumed to be known. For given values of f and ω , the only unknowns are the coefficients C'_u , C'_d , and C_d , which will be derived using the boundary conditions. The continuity of the displacement and stress vectors at $z = H$ and the vanishing of the stress vector at $z = 0$ give

$$C'_u e^{iHk\eta'} + C'_d e^{-iHk\eta'} = C_u e^{iHk\eta} + C_d e^{-iHk\eta}, \quad (\text{A10})$$

$$\frac{\mu' \eta'}{\mu \eta} (C'_u e^{iHk\eta'} - C'_d e^{-iHk\eta'}) = (C_u e^{iHk\eta} - C_d e^{-iHk\eta}), \quad (\text{A11})$$

$$C'_u = C'_d. \quad (\text{A12})$$

Using (A12), (A10) and (A11) can be rewritten as

$$2C'_u \cos\theta - C_d e^{-iHk\eta} = C_u e^{iHk\eta}, \quad (\text{A13})$$

$$2RiC'_u \sin\theta + C_d e^{-iHk\eta} = C_u e^{iHk\eta}, \quad (\text{A14})$$

where

$$\theta = Hk\eta', \quad (\text{15a})$$

$$R = \frac{\mu' \eta'}{\mu \eta}. \quad (\text{15b})$$

Solving the system of equations gives

$$C'_u = \frac{C_u e^{iHk\eta}}{\cos\theta + iR \sin\theta} \quad (\text{A16})$$

$$C_d = \frac{\cos\theta - iR \sin\theta}{\cos\theta + iR \sin\theta} C_u e^{2iHk\eta}. \quad (\text{A17})$$

The surface displacement, indicated with v'_0 , is obtained from (A6), (A12), and (A16) with $z = 0$:

$$v'_0 = 2C'_u e^{i(\omega t - kx)} = 2 \frac{C_u e^{iHk\eta}}{\cos\theta + iR \sin\theta} e^{i(\omega t - kx)}. \quad (\text{A18})$$

Equations similar to (A17) and (A18) are given by Haskell (1960) and Ben-Menahem and Singh (1981), but the former does not include the exponential factors involving H . We are interested in the amplitude of v'_0/C_u . If $\beta' < \beta$, then θ and R are real (because $c \geq \beta$). Therefore,

$$\left| \frac{v'_0}{C_u} \right| = \frac{2}{\sqrt{\cos^2\theta + R^2 \sin^2\theta}}. \quad (\text{A19})$$

To find out the extremal values of $|v'_0/C_u|$ set the derivative with respect to θ equal to zero, which gives

$$(1 - R^2) \sin 2\theta = 0. \quad (\text{A20})$$

This in turn implies that $\sin 2\theta = 0$ and

$$2\theta = \pi, 2\pi, \dots, m\pi, \dots, \quad (\text{A21})$$

where m is an integer.

For $R < 1$, if θ is an odd multiple of $\pi/2$, the right side of (A19) is equal to $2/R$, which is a maximum value (larger than 2). On the other hand, if θ is a multiple of π the right side of (A19) becomes 2, a minimum value. A similar argument shows that when $R > 1$ the maximum value is 2 and the minimum value is $2/R$.

It is useful to express (A20) in terms of the period T for which $|v'_0/C_u|$ is maximum:

$$\theta = Hk\eta' = H \frac{\omega}{c} \eta' = \frac{2}{Tc} \pi H\eta' = (2n + 1) \frac{\pi}{2}; \quad n = 0, 1, 2, \dots \quad (\text{A22})$$

Therefore,

$$T = \frac{4H\eta'}{(2n + 1)c}. \quad (\text{A23})$$

For the case of normal incidence $f = f' = 0$ and $c = \infty$. For this reason the previous equations cannot be used di-

rectly, and a limiting approach is needed. Since c is larger than β and β' , from (A5a) and an equivalent expression for η we see that

$$\eta' = \frac{c}{\beta}, \quad (\text{A24a})$$

$$\eta = \frac{c}{\beta} \quad (\text{A24b})$$

in the limit as c goes to infinity. Therefore, the ground displacement becomes

$$v'_0 = 2C'_u e^{i\omega t} = 2 \frac{C_u e^{iH\omega/\beta}}{\cos\theta + iR\sin\theta} e^{i\omega t} \quad (\text{A25})$$

with

$$\theta = \frac{Hkc}{\beta'} = \frac{H\omega}{\beta'}. \quad (\text{A26})$$

Introducing (A24a) in (A23) gives

$$T_m = \frac{4H}{(2n + 1)\beta'}. \quad (\text{A27})$$

Similarly, from (A15b)

$$R = \frac{\mu'\beta}{\mu\beta'} = \frac{\rho'\beta'}{\rho\beta} \quad (\text{A28})$$

and

$$\max \left| \frac{v'_0}{C_u} \right| = \frac{2}{R} = 2 \frac{\rho\beta}{\rho'\beta'}. \quad (\text{A29})$$

When $\beta = \beta'$ and $\rho' = \rho$, the maximum value is 2. Therefore, the amplification of the ground motion due to the presence of the layer is given by

$$A = \frac{\rho\beta}{\rho'\beta'} \quad (\text{A30})$$

(Kanai, 1957). Equation (A27) can be recast in terms of the wavelength λ'_m , which is equal to $T_m\beta'$:

$$\lambda'_m = \frac{4H}{2n + 1}. \quad (\text{A31})$$

When $n = 0$, (A31) gives

$$H = \frac{1}{4} \lambda'_m. \quad (\text{A32})$$

Equation (A32) corresponds to the well-known quarter-wavelength rule for the thickness of the layer, which only applies in the case of normal incidence. An early application of this rule was by Wiechert, who used it to determine the thickness of the soil in Göttingen, Germany, from the period of a teleseismic recording and the velocity of the S waves (Wiechert and Zoeppritz, 1907).

As an aside, it is worth noting that some authors use \sqrt{A} instead of A as the amplification factor. This factor derives from ray theory considerations and is widely used in seismic risk studies in connection with the quarter-wavelength rule. However, because a ray theory argument precludes the presence of layers, the concept of a preferred wavelength is nonphysical. On the other hand, according to Boore and Brown (1998), \sqrt{A} is the root mean square of $|v'_0/C_u|$ as a function of frequency, which makes this factor more physical, although it obviously underestimates the true values of the peak amplitudes.

Finally, the effect of attenuation in the layer is considered. One way to introduce it is to use a complex velocity, with β' replaced by

$$\beta' \left(1 + \frac{1}{2Q}i \right). \quad (\text{A33})$$

If desired, a similar equation can be used for the half-space. This approach, however, does not include the dispersion that accompanies attenuation (Ganley, 1981).

Center for Earthquake Research and Information
The University of Memphis
Memphis, Tennessee 38152
(J.P.)

Department of Civil Engineering
The University of Memphis
Memphis, Tennessee 38152
(S.P.)

Department of Petroleum and Geosystems Engineering
The University of Texas
CPE 2.502
Austin, Texas 78712
(Y.Z.)

Department of Civil Engineering
Northern Jiaotong University
Beijing 100044, P.R. China
(C.Z.)